THE JOURNAL OF PHYSICAL CHEMISTRY B

Article

pubs.acs.org/JPCB

Whole Ribosome NMR: Dipolar Couplings and Contributions to Whole Cells

Published as part of The Journal of Physical Chemistry virtual special issue "Recent Advances in Connecting Structure, Dynamics, and Function of Biomolecules by NMR".

Rie Nygaard,[†,‡] Joseph A. H. Romaniuk,[†] David M. Rice,[§] and Lynette Cegelski*

Department of Chemistry, Stanford University, 380 Roth Way, Stanford California 94305, United States

ABSTRACT: Solid-state NMR is a powerful tool for quantifying chemical composition and structure in complex assemblies and even whole cells. We employed N{P} REDOR NMR to obtain atomic-level distance propensities in intact ^{15}N-labeled *E. coli* ribosomes. The experimental REDOR dephasing of shift-resolved lysyl amine nitrogens by phosphorus was comparable to that expected from a calculation of N−P distances involving the lysines included in the crystal structure coordinates. Among the nitrogen contributions to the REDOR spectra, the strongest dephasing emerged from the dipolar couplings to phosphorus involving nitrogen peaks ascribed primarily to rRNA, and the weakest dephasing arose from protein amide nitrogens. This approach is applicable to any macromolecular system and provides quantitative comparisons of distance proximities between shift-resolved nuclei of one type and heteronuclear dephasing spins. Enhanced molecular specificity could be achieved through the use of spectroscopic filters or specific labeling. Furthermore, ribosome ^{13}C and ^{15}N CPMAS spectra were compared with those of whole cells from which the ribosomes were isolated. Whole-cell signatures of ribosomes were identified and should be of value in comparing overall cellular ribosome content in whole-cell samples.

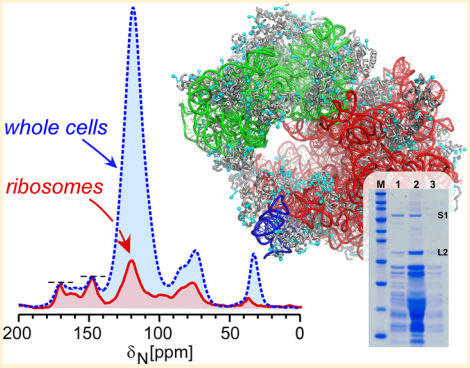

INTRODUCTION

The ribosome is the ultimate cellular machine. Ribosomes are made up of ribosomal RNA (rRNA) and over 50 proteins in bacteria, organized into large and small subunits, to translate genetic instructions into proteins. Tremendous contributions over decades have transformed early electron microscopy images and plaster of Paris models of the glove-like assembly[1] into high-resolution atomic-level coordinates through X-ray crystal structure determinations and, more recently, through cryo-electron microscopy (EM). High-resolution structures are now available for many ribosomes purified from bacteria, including *Haloarcula marismortui* (the first 50S subunit structure published in 2000),[2] *Thermus thermophilus*,[3] *E. coli*,[4] *B. subtilis*,[5] and *Mycobacterium smegmatis*.[6] The first eukaryotic ribosome was determined for the yeast *Saccharomyces cerevisiae* in 2010.[7] Since then, cryo-EM structures with 2.5−5 Å resolution have been reported for the 80S ribosomes from human,[8] *Drosophila*,[9] *Plasmodium falciparum*,[10] and *Trypanosoma cruzi*[11] and for the mammalian mitochondrial and spinach chloroplast ribosomes.[12,13]

These structures have yielded invaluable insight into ribosome function and the modes of action of ribosome-targeting antibiotics. New ribosome structures continue to be determined from other species and domains of life, revealing major similarities but also structural differences.[14,15] Differences in ribosome structures across kingdoms, for example, enable the use of ribosome-targeting antimicrobials to arrest bacterial protein synthesis while not significantly affecting human ribosome function. Computational studies have sought to examine and understand the statistical propensity of various amino acids involved in protein−RNA contacts lending structural integrity to ribosomes and other protein−RNA complexes, often by examining dozens of available and relevant crystal structures of certain types.[16,17] Yet, within available structures, electron density can be missing or imprecise near protein side chains.

We demonstrate that important atomic-level distance propensities can be obtained for intact ribosomes using rotational-echo double resonance (REDOR) solid-state NMR.[18] REDOR NMR is uniquely suited to determining individual and site-specific internuclear distances within biological assemblies as well as measuring the collective proximities between a certain type of nucleus distributed over many sites and dephasing spins to capture propensities of contacts or distance distributions.[19] For example, a 1.1 ms C{N} REDOR experiment can identify all carbons in a sample that are bonded to N and provides the percent of carbons at a specified chemical shift in that one-bond contact distance. Longer

Received: July 10, 2017
Revised: September 12, 2017
Published: September 13, 2017

DOI: 10.1021/acs.jpcb.7b06736
J. Phys. Chem. B 2017, 121, 9331−9335

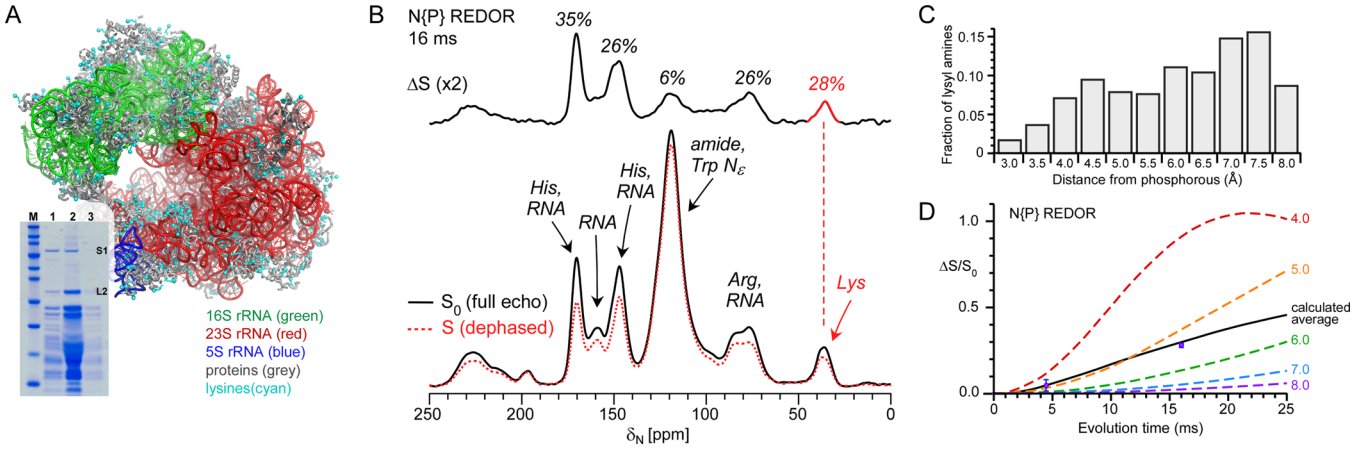

Figure 1. Whole ribosome NMR. (A) View of the ribosome crystal structure (PDB 4V4Q),[4] highlighting lysines in cyan and ε-nitrogen atoms of all of the lysines as cyan spheres. SDS-PAGE characterization verified the integrity of the uniformly ^{15}N-labeled ribosome preparation, with lanes M (markers), 1 (ribosome standard, New England Biolabs), 2 (^{15}N-labeled ribosomes), and 3 (1:10 dilution of ^{15}N-labeled ribosomes). (B) N{P} REDOR spectra obtained for a 16 ms evolution time reveals percent dephasing of nitrogens near to phosphorus. (C) Distribution of lysyl amine to phosphorus contacts for lysines present in the ribosome crystal structure. (D) REDOR $\Delta S/S_0$ values for 4.48 and 16 ms evolution times are 0.05 ± 0.03 and 0.263 ± 0.009, respectively, and fit well to the calculated REDOR curve corresponding to the distribution of binned distances from panel C (solid black). Representative single-distance REDOR curves are provided for comparison (dashed).

distances are measured and evaluated by increasing the REDOR evolution time for the experiment. The approach does not require crystalline material, and REDOR measurements have been made in purified proteins and enzymes, in bacterial whole cells, and even in intact plant leaves.[19] Atomic-level detail for DNA packaging in bacteriophage T4 capsids employed N{P} REDOR to describe the electrostatic interactions and mechanisms for DNA charge balance in capsid packaging.[20] Furthermore, we have been developing approaches to identify and compare spectral signatures of specific biomolecules in the context of intact whole cells.[21−24] For example, we were able to distinguish whether bacteria were treated with a cell-wall-targeting antibiotic (fosfomycin) or a protein synthesis inhibitor targeting the ribosome (chloramphenicol) by inspecting the natural abundance ^{13}C NMR spectra of antibiotic-treated whole cells.[22]

Here, we introduce a REDOR approach to evaluate the total collection of lysine−RNA proximities in intact ribosomes from *E. coli*. We performed N{P} REDOR NMR on uniformly ^{15}N-labeled ribosomes to measure the spectral dephasing of shift-resolved lysyl amines by rRNA phosphates and report on the collective dipolar couplings between [ε-^{15}N]Lys and ^{31}P nuclei. Results are compared with expectations from the available proximities in the X-ray crystal structure (Figure 1A). REDOR dephasing of other nitrogens in the system, including rRNA and protein amides, provides internal comparisons for relative distance propensities. Additionally, with approximately 20 000 ribosomes per bacterium, ribosomes can account for up to one-fourth of the dry mass of the cell.[25] We compared ^{13}C and ^{15}N NMR spectra of ribosomes with whole-cell spectra and identified spectral signatures of ribosomes that could be valuable in comparing ribosome content even in unperturbed whole-cell samples.

MATERIALS AND METHODS

Ribosome and Whole-Cell Sample Preparation. Both whole-cell and ribosome samples for NMR analysis were extracted from *E. coli* grown in M9 minimal media with [^{15}N]NH_4Cl (98% ^{15}N enrichment) and/or [$^{13}C_6$]glucose (99% ^{13}C enrichment) to yield uniformly ^{15}N-labeled ribosomes or ^{13}C- and ^{15}N-labeled whole-cell samples. To ensure complete labeling, a culture of *E. coli* MRE-600 was started in LB broth and grown overnight, diluted 1:100 in an M9 medium and grown to midexponential phase and then further diluted 1:50 in an M9 medium to prepare another overnight culture. This overnight culture was diluted 1:500, grown to an optical density of 0.60 at 600 nm, harvested by centrifugation at 10 000*g* for 4 min at 4 °C, and washed twice in ice-cold 5 mM HEPES, pH 7.4. For whole-cell samples, these cell pellets were frozen with liquid nitrogen and lyophilized.

For purification of ribosomes, the cell pellets were resuspended in 20 mL of lysis buffer (70 mM KCl, 10 mM $MgCl_2$, 10 mM Tris-HCl pH 7.4, PMSF and DNase (10 μg/mL)) and disrupted with 0.1 μm glass beads for three cycles of 1 min disruption and 1 min cooling on ice. The lysed cells were washed with 5 mM HEPES, centrifuged for collection, and filtered prior to loading onto an 8 mL Monolith column45 (CIMmultus QA-8 Advanced Composite Column (Quarternary amine)) from BIA Separations for purification by FPLC.[26] A pure ribosome sample was obtained with elution at 450−550 mM NH_4Cl. The ribosome fractions were combined, concentrated, and exchanged into lyophilization buffer (5 mM HEPES, 0.5% PEG-8000, and 30 mM trehalose). The purification resulted in greater than 10 mg of ribosomes per liter of bacterial cell culture.

Solid-State NMR and REDOR. Solid-state CPMAS[27] and N{P} REDOR NMR were employed in this study. REDOR NMR enables the measurement of heteronuclear dipolar couplings between heteronuclear spin pairs.[18] The dipole−dipole coupling between heteronuclei within a magnetic field is dependent upon both spatial and spin coordinates. Magic-angle spinning averages over the spin coordinates and suppresses the dipolar interactions in a coherent manner. The REDOR measurement utilizes the application of rotor-synchronized radio frequency pulses to operate exclusively on the spin coordinates and interferes with the complete suppression of the dipolar coupling by magic-angle spinning. This recoupling, or reintroduction of the dipolar coupling, enables the measurement of dipolar couplings and hence distances. The ^{15}N{^{31}P}

DOI: 10.1021/acs.jpcb.7b06736
J. Phys. Chem. B 2017, 121, 9331−9335

REDOR dephasing of the lysyl peak is reported as the experimental dephasing ($\Delta S/S_0$) for two REDOR evolution times (4.48 and 16 ms). The ΔS value was calculated from the difference in peak heights of the lysyl peak in the S_0 and S spectra. Experimental uncertainties are represented with error bars. Error bars were calculated by measuring the standard deviations of the noise in a signal-free region of the spectra (−200 to −400 ppm) and propagating the error through the ΔS and $\Delta S/S_0$ calculations.[28] Specifically, the error/uncertainty of ΔS is the $\sqrt{([\text{error in } S_0]^2 + [\text{error in } S]^2}$. NMR data were processed in vnmrj 4.0 and using custom scripts in Matlab.

All NMR experiments were performed in an 89 mm bore 11.7 T magnet (Agilent Technologies, Danbury CT) using a home-built four-frequency HPCN transmission line probe (^{1}H 500.92 MHz, ^{31}P 202.78 MHz, ^{13}C 125.96 MHz, and ^{15}N 50.76 MHz) with a four-channel DD2 console (Agilent Technologies), employing high-power linear transmitter/receiver (T/R) line switching on the ^{13}C channel and a passive diode preamp on the ^{15}N channel. Samples were spun at 8000 or 7143 Hz in thin-wall 5 mm zirconia rotors and maintained at −5 °C with an FTS chiller (FTS Thermal Products, SP Scientific, Warminster, PA) supplying nitrogen at −25 °C. Field strengths for ^{13}C and ^{15}N cross-polarization were all 50 kHz with a 10% ^{1}H linear ramp centered at 57 kHz. The echo-detection and REDOR π pulses were all 10 μs (for ^{15}N and ^{31}P), and SPINAL ^{1}H decoupling was applied at 72 kHz during acquisition and at 100 kHz during REDOR periods. The CPMAS mixing time was 1.5 ms, and the recycle time was 3.0 s for all experiments. ^{13}C chemical shifts were referenced to tetramethylsilane as 0 ppm using a solid adamantine sample at 38.5 ppm. The ^{15}N chemical shift scale was referenced to ammonia at 0 ppm where solid L-[amide-^{15}N]Asn appears at 114.5 ppm. Referencing to ammonia at 0 ppm is a change from some previous uses of solid NH_4SO_4 for which L-[amide-^{15}N]Asn would be reported as 89.1 ppm. The 4.4 ms (32 T_r) evolution time N{P} REDOR measurement was performed with 7143 Hz magic-angle spinning, and the 16 ms (128 T_r) evolution time N{P} REDOR measurement was performed with 8000 Hz magic-angle spinning.

RESULTS

Biochemical Characterization of Purified Ribosomes. Isotopically labeled ribosomes were purified from *E. coli* MRE600, the strain from which ribosomes were purified for the crystal structure determination reported in 2005.[4] Specifically, ribosomes were isolated from bacteria harvested at OD_{600} of 0.6, purified using a Monolith chromatography column, and analyzed by UV−vis spectrophotometry and protein gel electrophoresis. The 280/260 nm absorbance ratio was greater than 1.8, consistent with the RNA-to-protein ratio for an intact ribosome sample. The purified ribosome preparation was also compared with a commercially available *E. coli* ribosome standard (New England Biolabs 70S ribosomes) by protein gel electrophoresis and confirmed the integrity of the ribosomes in having the correct protein profile (Figure 1A).

REDOR for Ribosomes. N{P} REDOR was employed to determine the experimental dephasing of ribosomal nitrogens by phosphates in rRNA using uniformly ^{15}N-labeled ribosomes. Lysine side-chain nitrogens are resolved from other amino acid side-chain nitrogens and RNA nitrogens, whereas histidine and arginine side chains overlap with RNA nitrogens (Figure 1B). Thus, we sought a quantitative analysis of lysine dephasing by phosphorus and considered dephasing of other nitrogens more holistically for potential comparative power in considering all nitrogens in the sample. We performed N−P REDOR NMR with evolution times of 4.4 and 16 ms. The 16 ms REDOR spectra yielded significant dephasing of nitrogen peaks and immediately revealed a wide range of average dipolar couplings between different types of nitrogens and rRNA in the ribosome. The lysine nitrogens exhibited 28% dephasing and will be considered further below in comparison with expectations from the crystal structure. RNA-only contributions dominate the spectrum between 140 and 180 ppm. This region also contains contributions from histidine nitrogens, but these are expected to be small based on CPMAS spectral intensities for other uniformly ^{15}N-labeled proteins.[29] More specifically, adenosine and guanosine position 9 nitrogens appear at 170 ppm and serve as the attachment point to the sugar ring with its monophosphate. As expected, dephasing of this peak was strong (35%) and should serve as an internal ruler for maximal dephasing in ribosome samples. In contrast, the protein amide peak exhibited the weakest dephasing by ^{31}P, with a $\Delta S/S_0$ of 6%. This minimal dephasing is consistent with the protein backbone amide nitrogens being more distant, on average, from phosphates than rRNA nitrogens. Dephasing of lysyl side-chain nitrogens was strong and exhibited a $\Delta S/S_0$ of 28%. We took the opportunity to consider the lysine dephasing in a more detailed manner in the context of ribosome structure.

E. coli ribosomes typically contain 55 proteins (22 in the small subunit and 33 in the large subunit) and three distinct rRNA strands (5S and 23S rRNA in the large subunit and 16S rRNA in the small subunit).[25] The total protein content includes 685 lysines. The crystal structure of the *E. coli* ribosome[4] included modeled density for 558 lysines. The difference from the total number of ribosome lysines is attributed to two sources: (i) 43 fewer lysines were included because the ribosomes used for crystallography were depleted of the S1 protein, and (ii) additional missing lysines were attributed to flexible proteins that were not included in the structure.[4] The proximities of all 558 lysines annotated in the crystal structure to phosphates were binned in 0.5 Å increments, resulting in the distance distribution presented in Figure 1C. The expected N{P} REDOR $\Delta S/S_0$ curve was calculated for the total collection of ribosomal lysine side-chain nitrogens with the proximities to ^{31}P nuclei as binned in the histogram (Figure 1D). Simulated REDOR curves for single ^{15}N−^{31}P distances are provided for comparison to illustrate how collections of dipolar couplings result in an appropriately weighted REDOR curve. Strong dipolar couplings (short distances) contribute to strong early dephasing and the rapid rise in the $\Delta S/S_0$ curve, whereas weaker dipolar couplings require longer evolution times in order to contribute to REDOR dephasing. Ultimately, all 558 lysines would be dephased by phosphorus in the sample, with the REDOR curve reaching a maximum plateau of 1.0.

The calculated curve predicted 30% dephasing for the lysyl nitrogen dephasing by phosphorus after 16 ms of evolution time (Figure 1D). We observed 28% dephasing, close to what was predicted from the X-ray structure. Technically, the observed dephasing of 28% is just under 30% and is consistent with the set of lysines not reported in the crystal structure as being farther away from phosphorus. An additional REDOR experiment was performed with a 4.4 ms evolution time and yielded 4.6% dephasing (Figure 1D). REDOR NMR captured

DOI: 10.1021/acs.jpcb.7b06736
J. Phys. Chem. B 2017, 121, 9331−9335

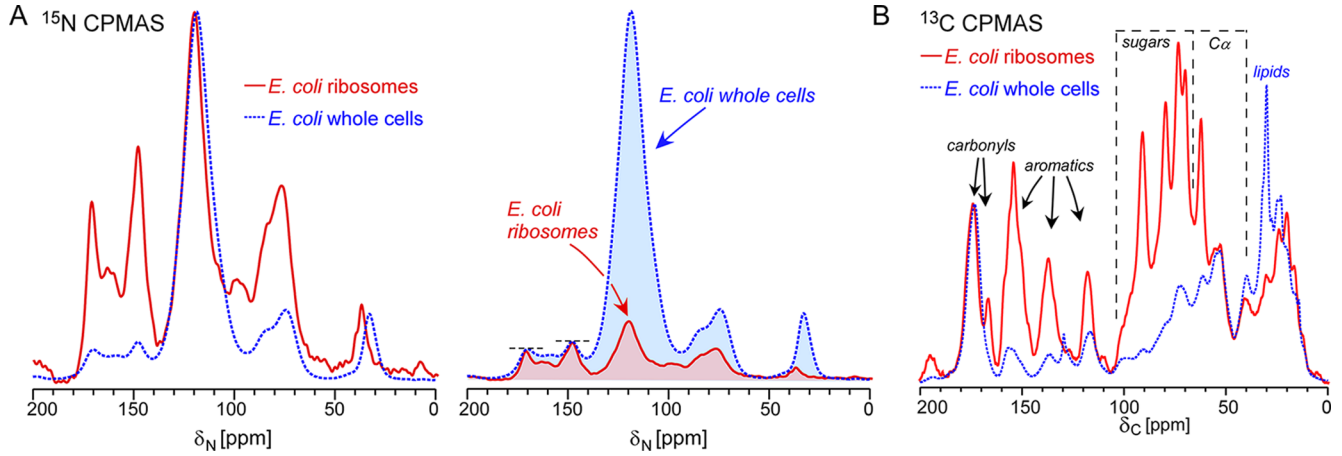

Figure 2. Whole ribosome and whole-cell NMR comparison. (A) ^{15}N CPMAS spectral overlays of purified ribosomes and the whole cells from which they were isolated (normalized to the nitrogen peptide peak at 120 ppm) demonstrate the dramatic differences in the nitrogen chemical composition of ribosomes versus that of whole cells (left). Scaling the ribosome spectrum to approximately match the whole-cell 147 and 170 peaks, given that the ribosome nitrogen peaks should be the dominant contributors in these regions, yielded a ribosome spectrum with 25% of the spectral area of the whole-cell spectrum (right). (B) A ^{13}C CPMAS spectral overlay of ribosomes and whole cells (normalized by the carbonyl peak height at 176 ppm) similarly reflects the dramatic carbon compositional differences, noting the enhanced ribosome intensity in aromatic and sugar carbons with respect to the carbonyl peak.

the distance distribution between all of the lysyl amine nitrogens and phosphates in purified ribosomes, without the need for crystalline preparations, and was comparable to the calculation based on the crystal structure. This approach could be employed to examine possible differences in the propensity of contacts among other prokaryotic and eukaryotic ribosomes. Furthermore, specific labeling with strategically selected ^{15}N-labeled amino acids could be employed to measure distance distributions between residues of interest and phosphates without overlapping contributions from other ribosome nitrogens. Such an approach would enable broad profiling and determination of the statistical propensity for side chains of arginines or histidines, for example, to be proximate to rRNA.

In addition to the specific analysis of N−P dipolar couplings, the one-dimensional REDOR spectra revealed the rich spectral profile of ribosomes that differs markedly from protein NMR and even whole-cell NMR spectra due to the unique RNA and protein composition of the ribosome. Thus, we took the opportunity to directly compare the ^{15}N and also ^{13}C NMR spectra of purified ribosomes with whole cells from which the ribosomes were purified.

NMR Comparisons of Nitrogen and Carbon Content in Ribosomes and Whole Cells. The N{P} REDOR full-echo S_0 spectrum revealed the unique nature of the ribosome nitrogen composition (Figure 1B). Nucleic acid ^{15}N peaks contribute significantly to the total ^{15}N spectral intensity of ribosomes and are salient features in a ribosome ^{15}N spectrum, readily distinguishing it from a typical protein or whole-cell NMR spectrum. Uniformly ^{15}N-labeled ribosomes and whole cells were first compared by ^{15}N cross-polarization magic-angle spinning (CPMAS) NMR. The two ^{15}N NMR spectra were normalized to the peptide backbone peak centered at 120 ppm to permit inspection of the relative content of RNA and nitrogen-containing side chains with respect to the protein amide content (Figure 2A, left). The much higher RNA-to-protein ratio in purified ribosomes is reflected in the CPMAS spectra, noting the major rRNA chemical shifts at 70−90 ppm and 147, 160, and 170 ppm. The lysyl amine nitrogen also exhibits a more downfield chemical shift than the average whole-cell amine peak (36 ppm in ribosomes), perhaps due to the propensity for lysine−phosphate hydrogen bonding in ribosomes. A comparison is also provided in which the ribosome and whole-cell spectra are scaled to match intensities in the salient rRNA peaks near 150 and 170 ppm (Figure 2A, right). On the basis of this scaling and taking into account sample masses, the ribosome spectrum accounts for approximately 25% of the integrated area of the whole-cell spectrum, consistent with the expected ribosome content in whole cells. Thus, comparisons of whole-cell ^{15}N NMR spectra may be of value in comparing ribosome status, by evaluating intensity changes in the 140−180 ppm peaks.

^{13}C CPMAS spectra of purified *E. coli* ribosomes and whole cells also revealed clear differences consistent with the compositional differences between the two systems. In whole cells, the carbonyl peak near 175 ppm is often used as the salient reference peak, and the lipid peak near 30 ppm is also usually an intense peak in the spectrum. All other carbon contributions in the cell are spread out over many different biomolecules, yielding broad spectral contributions through carbon chemical shifts between 10 and 180 ppm. In ribosomes, however, a unique ^{13}C spectrum is obtained, and the rRNA sugar peaks, which are detectable by ^{13}C NMR, are notably taller than the ribosome carbonyl peak. Collectively, these data emphasize how solid-state NMR can capture chemical composition noninvasively in intact systems and suggest that ^{15}N and ^{13}C whole-cell NMR should be of value in evaluating ribosome levels in intact cells.

CONCLUSIONS

Solid-state NMR can be recruited in many different ways to examine chemical composition and architecture in complex assemblies, regardless of size or complexity or potentially unknown components present. One can define and quantify the total collection of carbons and nitrogens at specified chemical shifts and, even more specifically, through spectral filters and specific labeling to resolve overlapping chemical shift contributions. Interest in quantification is a particular motivation for relying on one-dimensional NMR methods,

DOI: 10.1021/acs.jpcb.7b06736
J. Phys. Chem. B 2017, 121, 9331−9335

including REDOR, which enables quantitative accounting of dipolar couplings in a system. Here, we introduced a solid-state NMR approach to characterize chemical composition and intermolecular interactions in intact ribosomes purified from *E. coli*, without requiring any degradative or invasive analysis. We used this system as a model system, believing that the crystal structure coordinates should largely represent the relevant functional state for most of the ribosome. Dipolar couplings between lysyl amine nitrogens and rRNA phosphates were measured experimentally with REDOR NMR and were comparable to calculations derived from the X-ray structure coordinates. The REDOR measurements, however, did not require optimizations to prepare crystalline material, were performed on lyophilized ribosomes, and were not hindered by flexibility that could be present in solution and not captured in crystals. In addition, we took the opportunity to compare ribosome ^{13}C and ^{15}N CPMAS NMR spectra with whole-cell spectra and identified salient ribosome signatures that should be of future value in quantifying ribosome content or mapping interactions with ribosome-binding compounds in the context of intact whole cells.

AUTHOR INFORMATION

Corresponding Author

*E-mail: cegelski@stanford.edu. Telephone: 650-725-3527. Fax: 650-723-4817.

ORCID

Lynette Cegelski: 0000-0002-0978-1814

Present Addresses

‡R.N.: Department of Physiology and Cellular Biophysics, Columbia University, New York, NY 10027.

§D.M.R.: School of Natural Sciences, University of California Merced, CA 95340.

Author Contributions

†R.N. and J.A.H.R. contributed equally to this work.

Notes

The authors declare no competing financial interest.

ACKNOWLEDGMENTS

This material is based upon work supported by the National Science Foundation CAREER Award 1453247 (L.C.) and the National Institute of General Medical Sciences of the National Institutes of Health under Award Number R01GM117278 (L.C.). R.N. was supported by the Lundbeck Foundation Postdoctoral Fellowship.

REFERENCES

(1) Lake, J. A. Ribosome Structure Determined by Electron Microscopy of Escherichia coli Small Subunits, Large Subunits and Monomeric Ribosomes. *J. Mol. Biol.* **1976**, *105*, 131−139.

(2) Ban, N.; Nissen, P.; Hansen, J.; Moore, P.; Steitz, T. The Complete Atomic Structure of the Large Ribosomal Subunit at 2.4 Å Resolution. *Science* **2000**, *289*, 905−920.

(3) Ramakrishnan, V.; et al. Structure of the 30S Ribosomal Subunit. *Nature* **2000**, *407*, 327−339.

(4) Schuwirth, B. S.; Borovinskaya, M. A.; Hau, C. W.; Zhang, W.; Vila-Sanjurjo, A.; Holton, J. M.; Cate, J. H. D. Structures of the Bacterial Ribosome at 3.5 Angstrom Resolution. *Science* **2005**, *310*, 827−834.

(5) Beckert, B.; Abdelshahid, M.; Schafer, H.; Steinchen, W.; Arenz, S.; Berninghausen, O.; Beckmann, R.; Bange, G.; Turgay, K.; Wilson, D. N. Structure of the Bacillus subtilis hibernating 100S ribosome reveals the basis for 70S dimerization. *EMBO J.* **2017**, *36*, 2061.

(6) Hentschel, J.; Burnside, C.; Mignot, I.; Leibundgut, M.; Boehringer, D.; Ban, N. The Complete Structure of the Mycobacterium smegmatis 70S Ribosome. *Cell Rep.* **2017**, *20*, 149−160.

(7) Ben-Shem, A.; Jenner, L.; Yusupova, G.; Yusupov, M. Crystal Structure of the Eukaryotic Ribosome. *Science* **2010**, *330*, 1203−1209.

(8) Khatter, H.; Myasnikov, A. G.; Natchiar, S. K.; Klaholz, B. P. Structure of the Human 80S Ribosome. *Nature* **2015**, *520*, 640−645.

(9) Anger, A. M.; Armache, J. P.; Berninghausen, O.; Habeck, M.; Subklewe, M.; Wilson, D. N.; Beckmann, R. Structures of the Human and Drosophila 80S Ribosome. *Nature* **2013**, *497*, 80−85.

(10) Wong, W.; Bai, X. C.; Brown, A.; Fernandez, I. S.; Hanssen, E.; Condron, M.; Tan, Y. H.; Baum, J.; Scheres, S. H. Cryo-EM Structure of the Plasmodium falciparum 80S Ribosome Bound to the Anti-protozoan Drug Emetine. *eLife* **2014**, DOI: 10.7554/eLife.03080.

(11) Liu, Z.; Gutierrez-Vargas, C.; Wei, J.; Grassucci, R. A.; Sun, M.; Espina, N.; Madison-Antenucci, S.; Tong, L.; Frank, J. Determination of the Ribosome Structure to a Resolution of 2.5 Å by Single-Particle Cryo-EM. *Protein Sci.* **2017**, *26*, 82−92.

(12) Greber, B. J.; Boehringer, D.; Leibundgut, M.; Bieri, P.; Leitner, A.; Schmitz, N.; Aebersold, R.; Ban, N. The Complete Structure of the Large Subunit of the Mammalian Mitochondrial Ribosome. *Nature* **2014**, *515*, 283−286.

(13) Bieri, P.; Leibundgut, M.; Saurer, M.; Boehringer, D.; Ban, N. The Complete Structure of the Chloroplast 70S Ribosome in Complex with Translation Factor pY. *EMBO J.* **2017**, *36*, 475−486.

(14) Noller, H. F. RNA Structure: Reading the Ribosome. *Science* **2005**, *309*, 1508−1514.

(15) Moore, P. B. Structural Biology. A Ribosomal Coup: E. coli at Last! *Science* **2005**, *310*, 793−795.

(16) Bahadur, R. P.; Zacharias, M.; Janin, J. Dissecting Protein-RNA Recognition Sites. *Nucleic Acids Res.* **2008**, *36*, 2705−2716.

(17) Ellis, J. J.; Broom, M.; Jones, S. Protein-RNA Interactions: Structural Analysis and Functional Classes. *Proteins: Struct., Funct., Genet.* **2007**, *66*, 903−911.

(18) Gullion, T.; Schaefer, J. Rotational-Echo Double-Resonance NMR. *J. Magn. Reson.* **2011**, *213*, 413−417.

(19) Cegelski, L. REDOR NMR for Drug Discovery. *Bioorg. Med. Chem. Lett.* **2013**, *23*, 5767−5775.

(20) Yu, T. Y.; Schaefer, J. REDOR NMR Characterization of DNA Packaging in Bacteriophage T4. *J. Mol. Biol.* **2008**, *382*, 1031−1042.

(21) Romaniuk, J. A. H.; Cegelski, L. Bacterial Cell Wall Composition and the Influence of Antibiotics by Cell-Wall and Whole-Cell NMR. *Philos. Trans. R. Soc., B* **2015**, *370*, 20150024.

(22) Nygaard, R.; Romaniuk, J. A. H.; Rice, D. M.; Cegelski, L. Spectral Snapshots of Bacterial Cell-Wall Composition and the Influence of Antibiotics by Whole-Cell NMR. *Biophys. J.* **2015**, *108*, 1380−1389.

(23) Rice, D. M.; Romaniuk, J. A. H.; Cegelski, L. Frequency-Selective REDOR and Spin-Diffusion Relays in Uniformly Labeled Whole Cells. *Solid State Nucl. Magn. Reson.* **2015**, *72*, 132−139.

(24) Zhou, X.; Cegelski, L. Nutrient-Dependent Structural Changes in *S. aureus* Peptidoglycan Revealed by Solid-State NMR Spectroscopy. *Biochemistry* **2012**, *51*, 8143−8153.

(25) Nierhaus, K. H. Structure, Assembly, and Function of Ribosomes. *Curr. Top. Microbiol. Immunol.* **1982**, *97*, 81−155.

(26) Trauner, A.; Bennett, M. H.; Williams, H. D. Isolation of Bacterial Ribosomes with Monolith Chromatography. *PLoS One* **2011**, *6* (2), e16273.

(27) Schaefer, J.; Stejskal, E. O. C-13 Nuclear Magnetic-Resonance of Polymers Spinning at Magic Angle. *J. Am. Chem. Soc.* **1976**, *98*, 1031−1032.

(28) Kovacs, F. A.; Fowler, D. J.; Gallagher, G. J.; Thompson, L. K. A Practical Guide for Solid-state NMR Distance Measurements in Proteins. *Concepts Magn. Reson., Part A* **2007**, *30A*, 21−39.

(29) McDowell, L. M.; Schmidt, A.; Cohen, E. R.; Studelska, D. R.; Schaefer, J. Structural Constraints on the Ternary Complex of 5-enolpyruvylshikimate-3-phosphate Synthase from Rotational-Echo Double-Resonance NMR. *J. Mol. Biol.* **1996**, *256*, 160−171.

DOI: 10.1021/acs.jpcb.7b06736
J. Phys. Chem. B 2017, 121, 9331−9335